Pressure-induced antifluorite-to-anticotunnite phase transition in lithium oxide

A. Lazicki,[1,2] C.-S. Yoo,[1] W. J. Evans,[1] and W. E. Pickett[2]
[1]*Lawrence Livermore National Laboratory, Livermore, California 94550, USA*
[2]*Physics Department, University of California, Davis, California 95616, USA*
(Received 30 December 2005; published 22 May 2006)

Using synchrotron angle-dispersive x-ray diffraction and Raman spectroscopy on samples of Li_2O pressurized in a diamond anvil cell, we observed a reversible phase change from the cubic antifluorite (α, Fm-3m) to orthorhombic anticotunnite (β, Pnma) phase at 50(±5) GPa at ambient temperature. This transition is accompanied by a relatively large volume collapse of 5.4 (±0.8)% and large hysteresis upon pressure reversal (P_{down} at ~25 GPa). Contrary to a recent study, our data suggest that the high-pressure β-phase (B_o=188±12 GPa) is substantially stiffer than the low-pressure α-phase (B_o=90±1 GPa). A relatively strong and pressure-dependent preferred orientation in β-Li_2O is observed. The present result is in accordance with the systematic behavior of antifluorite-to-anticotunnite phase transitions occurring in the alkali-metal sulfides.

DOI: 10.1103/PhysRevB.73.184120 PACS number(s): 62.50.+p, 64.70.Kb, 64.30.+t

I. INTRODUCTION

Lithium oxide (Li_2O) is one of the simplest ionic oxides and it is isoelectronic to H_2O. At ambient pressure it exists in the antifluorite structure,[1] characterized by oxygen (O^{2-}) ions arranged in an fcc sublattice with lithium (Li^{1+}) ions in tetrahedral interstitial sites [Fig. 1(a)]. This structure is in contrast to that of isovalent symmetric ice (ice X), where the oxygen sublattice forms a bcc arrangement.[2] However, a further transformation to an antifluorite phase in ice at some pressure above 150 GPa has been predicted,[3,4] and experiments show changes in vibrational mode coupling[5] and single-crystal x-ray diffraction peak intensity[7] near 150 GPa. Recent studies argue that a new phase is either hexagonal or orthorhombic,[6] but the existence and nature of this phase and the pressure at which it is reached are still uncertain.[7,8] In further similarity to ice, for which a high-pressure, high-temperature superionic phase has been predicted,[9] ambient pressure Li_2O becomes superionic at temperatures above 1350 K,[10] prior to melting at 1705 K.[11] In the superionic phase, oxygen ions constitute a rigid framework while lithium ions move from one tetrahedral site to another via octahedral interstitial sites. Despite its marked similarities to H_2O, until very recently the high pressure behavior of Li_2O was not addressed in the literature. One report by Kunc *et al.*[12] identified a high pressure phase transition using powder x-ray diffraction and investigated trends under pressure using *ab initio* calculations, but so far data at only one pressure point in this high pressure phase has been reported.

Technological applications for this material range from possibilities for hydrogen storage (in combination with Li_3N[13]), to use as a blanket breeding material for thermonuclear reactors to convert energetic neutrons to usable heat and to breed tritium necessary to sustain deuterium-tritium reactions.[14,15] Understanding the behavior of Li_2O at high temperatures and pressures is, therefore, very useful for its applications as well as a potential aid in understanding the behavior of the hot, dense ice structures which are of such great importance to planetary science, geosciences, and fundamental chemistry. Additionally, investigation of this simple material is a reference point for understanding more complex metal-oxides.

In this study, we investigate the high pressure behavior of Li_2O at room temperature with angle-dispersive x-ray diffraction (ADXD) and Raman spectroscopy. We present further and more complete evidence for a phase transition from antifluorite to anticotunnite structure, recently observed for the first time by Kunc *et al.*,[12] and discuss it in light of similarities to trends observed in the alkali metal sulfides.

II. EXPERIMENT

Polycrystalline Li_2O powder (99.5% purity, CERAC, Inc.) was loaded into a membrane diamond anvil cell (DAC) of Livermore design. Brilliant cut diamonds with 0.3 mm flats were used with a 0.15 mm diameter sample chamber in a rhenium gasket of 0.05 mm initial thickness to achieve a pressure range of 8–61 GPa. No pressure medium was used in the experiments, as α-Li_2O has a low enough bulk modulus that nonhydrostaticity was not predicted to be a serious concern. This assumption turned out to be potentially problematic, as will be shown. In the first experiment copper was included in the sample chamber as an internal pressure indicator and in the second pressure was determined from micron-sized ruby (Al_2O_3:Cr^{3+}) crystals using the quasihy-

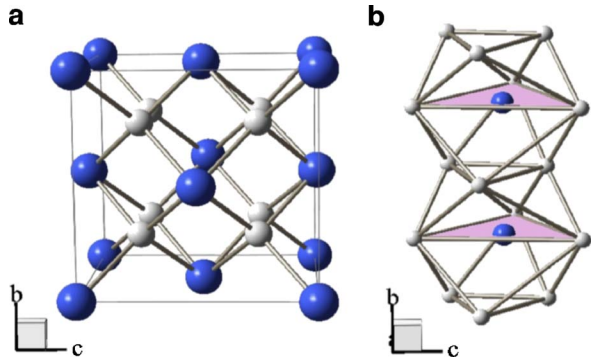

FIG. 1. (Color online) (a) antifluorite α-Li_2O structure. (b) Anticotunnite β-Li_2O structure showing the tri-capped trigonal prismatic coordination. Large atoms represent oxygen and smaller represent lithium.

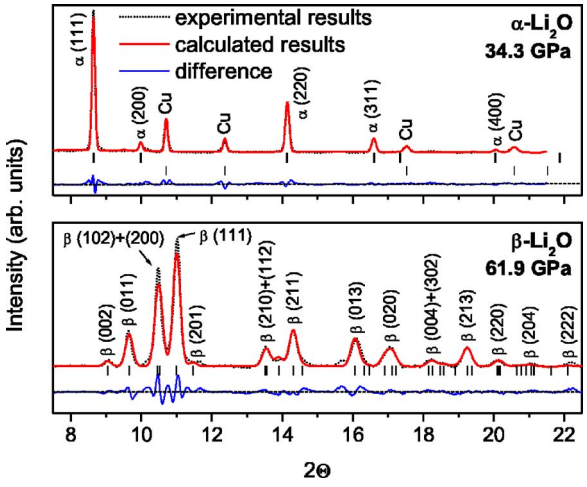

FIG. 2. (Color online) Rietveld refined x-ray diffraction profile of α- and β-Li_2O. For the diffraction patterns shown, the final refinement converged to $R(F^2)=0.1054$ for the α phase and $R(F^2)=0.1197$ for the β phase. In the high pressure phase, only the most intense reflections are labeled. Unit cell parameters for the phase were determined from the positions of the most isolated and/or intense peaks: (002), (011), (111), (211), (013), and (020).

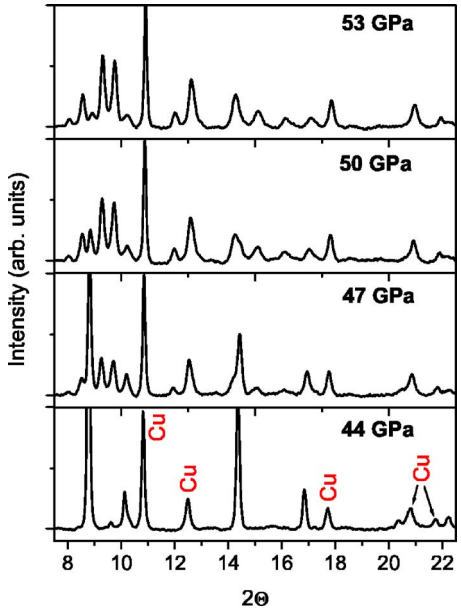

FIG. 3. (Color online) Li_2O ADXD patterns across the phase transition from cubic to orthorhombic, showing the large pressure range of two-phase coexistence.

drostatic ruby pressure scale.[16] All sample loadings were performed in an inert environment, as Li_2O is hygroscopic.

High-pressure behavior of Li_2O was investigated by ADXD and Raman spectroscopy, both at ambient temperature. ADXD was performed at the microdiffraction beamline 16IDB of the HPCAT (High Pressure Collaborative Access Team) at the APS (Advanced Photon Source). In these experiments, we used intense monochromatic x-rays ($\lambda=0.367\,98$ or $0.412\,85$ Å) microfocused to about 0.01 mm at the sample using a pair of piezo-crystal controlled bimorphic mirrors. The x-ray diffraction patterns were recorded on a high-resolution image plate detector (MAR 345). The recorded two-dimensional diffraction images (Debye-Scherrer rings) were then integrated to produce high quality ADXD patterns using FIT2D and analyzed with the XRDA[17] and GSAS (EXPGUI)[18] programs.

Raman spectra were excited using an argon-ion laser ($\lambda=514.5$ nm) focused to ~0.01 mm. Scattered light (measured in back-scattering geometry) was filtered with a 514.5 nm Super-Notch-Plus filter, analyzed with a single spectrometer (characterized by less than 3 cm^{-1} spectral resolution) consisting of a 1200 grooves/mm ion-etched blazed holographic diffraction grating, and imaged with a liquid nitrogen cooled CCD camera at Lawrence Livermore National Laboratory. A spectral range of 100–1400 cm^{-1} was used.

III. X-RAY DIFFRACTION

Rietveld refinements of the ADXD patterns of Li_2O confirm the identity of the antifluorite (α-Li_2O) structure (Fig. 2, top panel), which is found to be stable up to 45 GPa. Above this pressure, diffraction peaks from a new phase begin to emerge, as shown in Fig. 3. However, traces of the low-pressure phase are apparent up to nearly 55 GPa. This large coexistence region may be due to pressure gradients in the cell which arise because of a lack of pressure medium. However, all diffraction peaks remain relatively sharp across the transition, demonstrating that shear stress conditions are relatively uniform. In a homogeneous sample, such a coexistence region may be due to hysteresis arising from nucleation barriers to a first-order transition, or it may indicate that this transition is kinetically hindered or sluggish. These explanations seem more likely, and are consistent with an even larger (25 GPa) hysteresis that was observed upon pressure reversal, as will be shown.

The Cu pattern in the x-ray diffraction diagrams of Fig. 3 is undesirable for a clean refinement of crystal structure, particularly so for the high-pressure phase where several reflections from Cu overlap with those from the sample. We performed an additional experiment without Cu (but with ruby) and carried out a full Rietveld profile refinement of the structure based on the anticotunnite (β-Li_2O) structure ($PbCl_2$-type, Pnma, Z=4) identified in Ref. 12, and also seen in the similar alkali metal sulfide Li_2S system.[19] Clearly, the refined results (summarized in Fig. 2, lower panel) are reasonably good even at 61.9 GPa. The origin of the small reflection near $2\Theta=15.7$ is unknown, but does not originate from the sample. Refined parameters include cell parameters, profile function, fractional coordinates, thermal parameters, Chebyshev polynomial background, and the spherical harmonic (sixth-order) correction for preferred orientation (PO). The starting atomic coordinates were those determined for Li_2S in the Pnma structure at 7.9 GPa; $a=5.92$ Å, $b=3.65$ Å, $c=6.90$ Å, $x_O=0.77$, $x_{Li0}=0.98$, $x_{Li2}=0.32$, $z_O=0.61$, $z_{Li1}=0.36$, $z_{Li2}=0.56$. The final refinement converges to $R(F^2)=0.1197$, with atom positions given in Table I. At this pressure, a refinement of the PO correction yielded a texture index of 1.5437, indicating a moderate PO in the

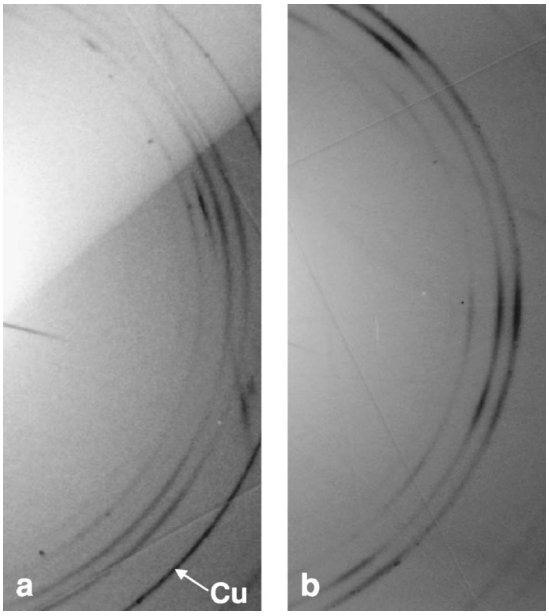

FIG. 4. Powder diffraction rings of β-Li_2O at 53 GPa (a) and 61 GPa (b), showing the presence of texture in this phase, and the increase in preferred orientation with pressure. The three most prominent rings shown are the (011), (102)+(200), and (111) reflections.

orthorhombic phase at 61.9 GPa (where a texture index value of 1.0 means no texture and 3.0 is strong texture). This effect is confirmed by the presence of clear intensity variations around the powder diffraction rings shown in Fig. 4. The PO appears to increase from 53 to 61 GPa (these patterns were, however, taken during separate experiments), an effect which may lead to the intensity inversion of the two most prominent peaks which is observed between 53 and 61 GPa in the diffraction spectra. Because of the quality of the data and relatively small number of diffraction peaks available, the refinement was not entirely conclusive, and the resulting structure must, therefore, be viewed as approximate.

The crystal structure of β-Li_2O can be understood to consist of chains of distorted tricapped trigonal prisms of cations parallel to the y-axis, giving the anion a coordination number of 9 [Fig. 1(b)]. Near the transition, the polyhedral cation-anion distances range from 1.664 to 2.246 Å with an average

TABLE I. Lattice parameters (given by XRDA) and refined fractional coordinates for β-Li_2O at 61.9 GPa. Uncertainties reported are those printed by GSAS for this refinement. However, the complexity of the structure and the quality of the data suggest that in reality these parameters are less certain.

Lattice parameters	a (Å)	b (Å)	c (Å)
(61.9 GPa)	4.456(2)	2.7865(6)	5.212(1)
Fractional coordinates	x	y	z
O	0.745(1)	0.25	0.600(1)
Li(1)	0.883(3)	0.25	0.305(2)
Li(2)	0.305(3)	0.25	0.570(3)

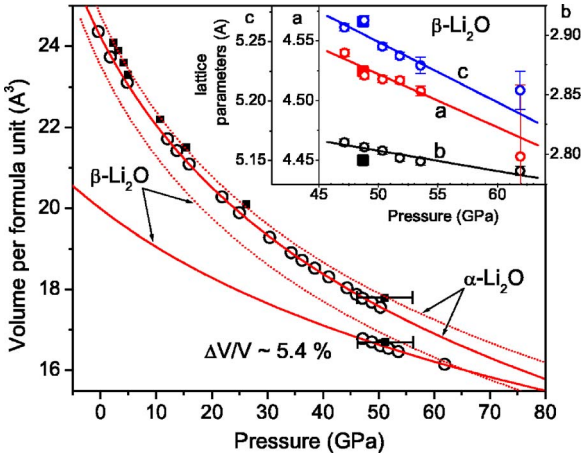

FIG. 5. (Color online) EOS for the two Li_2O phases. In the main plot, solid curves are the Birch-Murnaghan EOS fits to the experimental data (shown as open circles) in this study. Solid squares are the experimental data from Ref. 12 and dotted curves are the theoretically calculated EOS (Ref. 12) for both phases. Inset: Trends in the evolution with pressure of the lattice parameters in the β phase. Empty circles are data from this study (error bars shown when they exceed size of data points), and solid squares are experimental data from Ref. 12.

of 1.89 Å. These values are reasonable, based on the Li-O distances quoted for lithium oxide clusters in Ref. 20. In comparison, in the α-Li_2O structure, the anion coordination number is 8 with a cation-anion distance of 1.79 Å near the transition. There is a 5.4±0.3% volume collapse across the transition.

Figure 5 shows the pressure-volume data of the two phases, along with the best fit third-order Birch-Murnaghan equation of state (EOS) curves. Also shown are experimental data points and calculated EOS curves from Ref. 12. Fitting parameters are summarized in Table II. Because of a limited pressure range studied for β-Li_2O, it was necessary to constrain B' to equal 4. This approximation was based on the procedure adopted by Grzechnik *et al.*[19] in the case of Li_2S. Variation of this value between 3.5 and 4.5 resulted in at most a 12% difference in B_o and a 1% difference in V_o. The agreement between experimental and calculated equations of state for α-Li_2O suggest that pressure is reasonably hydrostatic in this phase. Contrary to the results of Kunc *et al.*,[12] under pressure we do not see major broadening of fluorescence line spectra from the ruby pressure calibrant in the α phase, an observation which could indicate that this phase supports substantial shear stress.

Although the single experimental data point shown for the high pressure β phase in Ref. 12, which was also acquired without a pressure medium, agrees well with the present work, there is a dramatic disparity between their calculated equation of state and the experimental one from this study. The β-Li_2O pressure-volume data from Ref. 12 are generated from *ab initio* total energy DFT calculations, using the projector augmented waves method. In the high pressure phase, the lattice constants and internal positions are determined by a process of "relaxing" these parameters, minimizing all forces at each step. In the experiment, however, the

TABLE II. Birch-Murnaghan EOS fitting parameters. Volumes are given per formula unit.

	B_o (GPa)		V_o (Å^3)		B'	
	This work	Ref. 12	This work	Ref. 12	This work	Ref. 12
α	90(1)	75(7)[a]	24.24(2)	24.69(9)[a]	3.51(5)	5.2(7)[a]
β	188(12)	80.8(18)[b]	20.0(2)	23.51(6)[b]	4 (fixed)	3.92(6)[b]

[a]Experimental results.
[b]Calculated results.

proposed increase in PO with pressure may suggest an increase in stress inhomogeneity as well, a highly nonhydrostatic state which is not well modeled by the relaxed structure in the calculation. The use of an optimally hydrostatic pressure medium in a future experiment may indicate just how well the theoretical model approximates reality in this case. It is doubtful that nonhydrostaticity alone can explain away the discrepancy, however. If the value for bulk modulus for the β phase were actually as close to that of the α phase as theory predicts, it is unlikely that nonhydrostatic effects would cause such a large "error" in the experimental equation of state of the β but not the α phase.

Although the dramatic factor-of-two increase in bulk modulus across this phase transition appears anomalously large, actually a similar (and larger) increase is recorded for the antifluorite-anticotunnite transition in Li_2S[19] and, although values for bulk modulus are not quoted, it appears that a similar effect is seen in Na_2S.[21] An examination of the pressure evolution of the a, b, and c lattice parameters, shown in the inset of Fig. 5, may explain the large increase in bulk modulus. We find that the b-axis is much stiffer (almost three times greater) than the a and c axes. Thus, the trigonal prism chains shown in Fig. 1(b) are seen to be very rigid and to strongly resist compression. This is consistent with the sizable directional effects which are apparent from the intensity variations of the diffraction rings in Fig. 4.

IV. RAMAN SPECTROSCOPY

The pressure-induced changes in Raman spectra of Li_2O give further evidence of a phase transition beginning near 49 GPa upon increasing pressure, as shown in Fig. 6. The low-pressure α phase has four formula units per unit cube. Factor group analysis gives one Raman active optical phonon mode T_{2g}, which describes motion of the Li sublattice. This mode is seen in the Raman spectrum near 575 cm^{-1} at low pressure. At the phase transition from α to β there is a considerable lowering of symmetry and consequently a significant increase in number of modes. The β phase has four formula units per unit cube, and factor group analysis yields $6A_g+3B_{1g}+6B_{2g}+3B_{3g}$ Raman active phonon modes. In the Raman spectrum of the β phase, we see three prominent bands (near 750, 800, and 830 cm^{-1}) and at least seven weaker bands at lower Raman shifts, not counting even weaker features appearing as shoulders of these bands. Since the sample is powder, a precise mode assignment for the Raman peaks is difficult. The observation of fewer modes than predicted by group theory is likely due to accidental degeneracy, insufficient instrumental resolution, and/or diminishingly weak intensity.

The pressure-induced shifts of the distinguishable Raman bands are plotted in Fig. 7, observed in both up (solid circles) and down (open circles) strokes of pressure. Experimental data and theory curves from Ref. 12 are also shown, for comparison. Data points are fit with an equation of state derived from valence force field theory which was previously shown to be physically realistic.[22] The frequency shifts with pressure of the individual bands and the corresponding mode grüneisen parameters are shown in Table III. The Raman band in the α phase shifts noticeably more rapidly than those in the β phase—a further confirmation of a large difference in bulk modulus. The dotted lines represent the approximate transition pressures upon increasing and decreasing pressure. There is a large (nearly 25 GPa) hysteresis in this transition (also seen from Fig. 6) and when decreasing pressure the $\beta \rightarrow \alpha$ transition occurs near 25 GPa. Several of the orthorhombic Raman bands can be seen to overlap and undergo changes in relative intensity in the pressure region between 25 and 45 GPa that is inaccessible when increasing pressure. Kunc *et al.*[12] observed a similar hysteresis and the data from their Raman experiment agrees well with the present study. Their calculated results (shown as dotted curves) for the α phase are also in very good agreement; the curve is almost perfectly aligned with our experimental data in that phase. The β phase calculated phonon mode shifts, however, show a marked disagreement. Nevertheless, this is not surprising as their EOS describes a much softer material

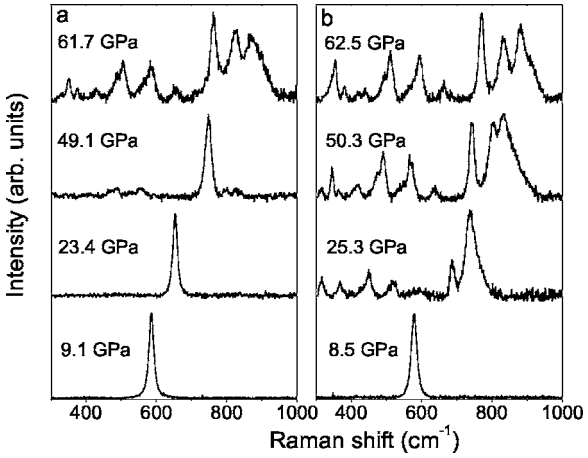

FIG. 6. Raman spectra upon increasing (a) and decreasing (b) pressure. Cosmic radiation spikes were removed from two of the spectra.

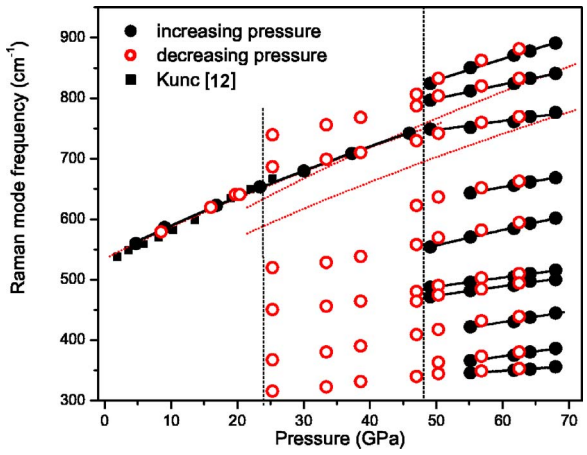

FIG. 7. (Color online) The shift in pressure of Li_2O Raman bands. Solid lines are fits to the experimental data from this study. Red dotted lines represent the calculated theoretical pressure dependence of the Raman frequencies from Ref. 12. In the cubic phase, the theoretical curve lines up exactly with the experimental result from this study. Vertical dashed lines approximate the phase transition pressure upon increasing and decreasing pressure.

with much more homogeneous stress conditions, so the Raman bands would be expected to occur at a lower frequency, and would shift more rapidly with pressure, as indeed the calculations predict.

V. DISCUSSION

The mechanism for the antifluorite-anticotunnite phase transition is already well understood because of the numerous well-known pressure-induced fluorite-cotunnite transitions that occur.[23,24] If one pictures the antifluorite structure as (111) planes of anions separated by pairs of (111) planes composed of ions from the cation sublattice, the mechanism for the transition can be seen as a displacement of the anions in the [111] directions, half to the adjacent upper plane and half to the adjacent lower plane, accompanied by rotations and distortions of the Li triangular polyhedra within the planes (Fig. 8). This transition has the advantage of increasing the oxygen coordination number from 8 to a more stable 9, increasing the average O-Li separation distance from 1.78 to 1.89 Å, and increasing the packing through the 5.4% volume collapse from 17.56 $Å^3$/formula unit to 16.61 $Å^3$/formula unit near 50 GPa. At this pressure, the α-Li_2O phase lattice parameter is a=4.126 Å while the β-Li_2O phase parameters are given by a=4.518 Å, b=2.808 Å, c=5.246 Å. Accompanying this transition is a remarkable 100 GPa increase in bulk modulus, for which an inhomogeneous stiffening of the material along the b-axis is at least partially responsible. The repulsion between closely spaced and highly charged ions also contributes to the overall stiffening of the crystal lattice, and threatens to destabilize the structure unless the coordination number is high around the most highly charged (O^{2-}) ions. Therefore, a transition to an Ni_2In-type structure is expected at higher pressure, as it would further increase the anion coordination number to 11.

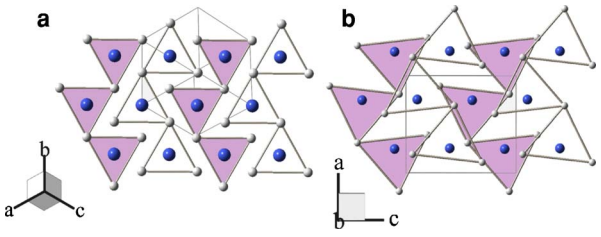

FIG. 8. (Color online) (a) α-Li_2O along the (111) plane, showing the transition mechanism to β-Li_2O (b). For the cubic structure shown in (a), all oxygen ions are coplanar, located midway between planes of lithium ions which are separated by 1.032 Å near 50 GPa. For the orthorhombic structure shown in (b), half the oxygen ions have moved into the lower plane of Li ions (shown as colored polyhedra) and half into the upper (empty), with the planes separated by 1.402 Å near 50 GPa.

TABLE III. Frequencies, pressure coefficients, and grüneisen parameters (all calculated at 50 GPa), for the plotted Raman modes of Li_2O.

Phase	ω (cm^{-1})	$\left[\frac{1}{\omega}\frac{d\omega}{dP}\right]$ (10^{-3} GPa^{-1})	γ
α-Li_2O	758	5.5(5)	1.3(1)
β-Li_2O	829	4.8(4)	1.8(2)
	799	3.4(4)	1.3(2)
	747	2.5(4)	0.9(2)
	632	3.7(4)	1.4(2)
	557	5.1(5)	1.9(2)
	488	3.6(4)	1.3(2)
	473	4(1)	1.4(2)
	411	5(1)	1.9(2)
	357	5.1(5)	1.9(2)
	342	2.7(8)	1.0(2)

An examination of the known behavior of alkali-metal chalcogenides under pressure may allow us to understand and predict the behavior of this class of materials. Although Li_2O is the first alkali-metal oxide which has been shown to possess a pressure-induced antifluorite-anticotunnite transition, it is common in alkali-metal sulfides.[19,21,25] Li_2S, Na_2S, K_2S, and Rb_2S have all been shown or are predicted to undergo an antifluorite to anticotunnite transition, at lower and lower pressures with increasing cation mass until, in Cs_2S, the anticotunnite phase is stable at ambient conditions (Fig. 9). These compounds are predicted to undergo a second transition from the anticotunnite to a hexagonal Ni_2In-type phase at even higher pressure[25] and so it is likely that Li_2O will do the same, although the calculations of Kunc *et al.*,[12] indicate that this will not occur below 100 GPa.

Alkali metal oxides K_2O, Na_2O, and Rb_2O also have the antifluorite structure at ambient conditions.[26,27] The only alkali metal oxide exception is Cs_2O, which has been seen to possess the $CdCl_2$ structure[28] which, however, is a simple rhombohedral distortion of the fluorite structure. No high-pressure studies have been performed on these materials, but

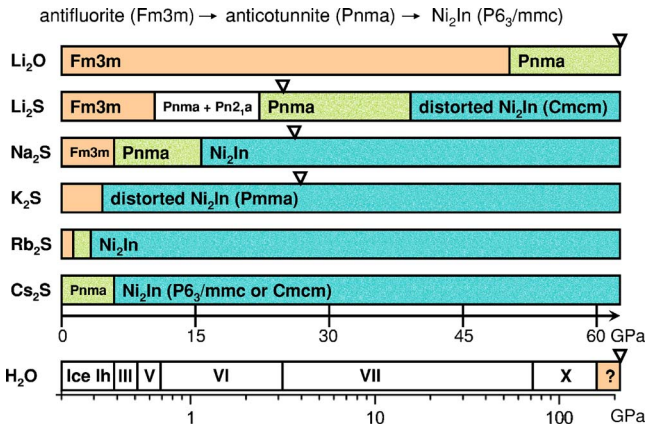

FIG. 9. (Color online) Comparison of Li_2O pressure behavior with that of the alkali-metal sulfides. H_2O may transition to a cubic antifluorite-type phase above 170 GPa, and, in the nonmolecular form, may be expected to follow the same trends as the alkali metal chalcogenides. ▽ represents the high pressure limit of experiments.

we can reasonably expect that they will follow the same series of transitions that have been observed here. Ice also, in the past, has been predicted to exist in the antifluorite structure at sufficiently high pressure.[3,4] Since then this proposition has been called into question, but the actual high pressure structure remains to be seen experimentally, and is most currently not predicted to exist below 170 GPa.[8] Ice VII gradually becomes "symmetric" ice-X at the pressure range of 40–90 GPa, with a bcc oxygen sublattice, similar to that of ice VII but with hydrogen atoms occupying the central position between adjacent oxygen atoms. The possibility of a transition of ice X to a phase similar to that of α-Li_2O could indicate a systematic pressure-induced structural behavior for all alkali-metal chalcogenides.

VI. CONCLUSION

A recently discovered pressure-induced antifluorite-anticotunnite phase transition, seen for the first time in an alkali-metal oxide,[12] was investigated in detail using x-ray diffraction and x-ray Raman scattering. Several new properties of the high pressure phase were discovered. A dramatic increase in bulk modulus was seen for the first time, and the source of the high pressure phase's rigidity identified to be related to an inhomogeneous stiffening of one of the crystal lattice parameters. A consequent preferred orientation which increases with pressure in the orthorhombic phase was identified as responsible for an inversion in the intensities of two of the most prominent x-ray diffraction peaks. The pressure-induced shift in the Raman bands of both phases was observed, and found to be consistent with our observation of a large bulk modulus increase. The x-ray diffraction and Raman data both point towards a strong hysteresis across this transition, which is consistent with a kinetically hindered or sluggish first-order transition, or one in which a large volume change and a large change in bulk modulus can serve as nucleation barriers for the transition. Comparisons were drawn between Li_2O and a series of alkali metal sulfides, allowing us to make confident predictions about the high pressure behavior of the rest of the alkali-metal chalcogenides and even, perhaps, the behavior of dense, nonmolecular ice at ultrahigh pressures.

ACKNOWLEDGMENTS

We would like to thank J. P. Klepeis for many helpful discussions. This work has been supported by the LLNL, University of California, under the auspices of the U.S. DOE under Contract No. W-7405-ENG-48 and by the Stewardship Science Academic Alliances Program under Grant No. DOE 01-06NA26204. Use of the HPCAT facility was supported by DOE-BES, DOE-NNSA (CDAC, LLNL, UNLV), NSF, DOD-TACOM, and the W. M. Keck Foundation. We thank HPCAT beamline scientist Maddury Somayazulu for technical assistance.

[1] *Constitution of Binary Alloys*, 2nd Suppl., edited by F. A. Shunk (McGraw-Hill, New York, 1969).
[2] K. R. Hirsh and W. B. Holzapfel, Phys. Lett. **101A**, 142 (1984).
[3] P. Demontis, R. LeSar, and M. L. Klein, Phys. Rev. Lett. **60**, 2284 (1988).
[4] P. Demontis, M. L. Klein, and R. LeSar, Phys. Rev. B **40**, 2716 (1989).
[5] A. F. Goncharov, V. V. Struzhkin, M. S. Somayazulu, R. J. Hemley, and H. K. Mao, Science **273**, 218 (1996).
[6] M. Benoit, M. Bernasconi, P. Focher, and M. Parrinello, Phys. Rev. Lett. **76**, 2934 (1996).
[7] P. Loubeyre, R. LeToullec, E. Wolanin, M. Hanfland, and D. Hausermann, Nature (London) **397**, 503 (1999).
[8] M. Benoit, A. H. Romero, and D. Marx, Phys. Rev. Lett. **89**, 145501–1 (2002).
[9] C. Cavazzoni, G. L. Chiarotti, S. Scandolo, E. Tosatti, M. Bernasconi, and M. Parrinello, Science **283**, 44 (1999).
[10] S. Hull, T. W. D. Farley, W. Hayes, and M. T. Hutchings, J. Nucl. Mater. **160**, 125 (1988).
[11] Y. Y. Liu, M. C. Billone, A. K. Fischer, S. W. Tam, and R. G. Clemmer, Fusion Technol. **8**, 1970 (1985).
[12] K. Kunc, I. Loa, A. Grzechnik, and K. Syassen, Phys. Status Solidi B **242**, 1857 (2005).
[13] Y. H. Hu and E. Ruckenstein, Ind. Eng. Chem. Res. **43**, 2464 (2004).
[14] S. Tanaka, M. Taniguchi, and H. Tanigawa, J. Nucl. Mater. **283-287**, 1405 (2000).
[15] K. Noda, K. Uchida, T. Tanifuji, and S. Nasu, Phys. Rev. B **24**, 3736 (1981).
[16] H. K. Mao, J. Xu, and P. M. Bell, J. Geophys. Res. **91**, 4673 (1986).
[17] S. Desgreniers and K. Lagarec, J. Appl. Crystallogr. **31**, 109 (1998).
[18] B. H. Toby, J. Appl. Crystallogr. **34**, 210 (2001).

[19] A. Grzechnik, A. Vegas, K. Syassen, I. Loa, M. Hanfland, and M. Jansen, J. Solid State Chem. **154**, 603 (2000).
[20] F. Finocchi and C. Noguera, Phys. Rev. B **53**, 4989 (1996).
[21] A. Vegas, A. Grzechnik, K. Syassen, I. Loa, M. Hanfland and M. Jansen, Acta Crystallogr., Sect. B: Struct. Sci. **57**, 151 (2001).
[22] W. A. Van Uden, H. Hubel, J. M. Hayes, A. D. Prins, M. Kuball, D. J. Dunstan, J. R. Downes, Y. Ying Shi, and J. H. Edgar, High Press. Res. **22**, 27 (2002).
[23] L. Gerwald, J. S. Olsen, S. Steenstrup, M. Malinowski, S. Åsbrink, and A. Waskowska, J. Appl. Crystallogr. **25**, 578 (1992).
[24] J. M. Leger, J. Haines, A. Atouf, O. Schulte, and S. Hull, Phys. Rev. B **52**, 13247 (1995).
[25] J. C. Schön, Ž. Čančareić, and M. Jansen, J. Chem. Phys. **212**, 2289 (2004).
[26] R. Dovesi, C. Roetti, C. Freyria-Fava, M. Prencipe, and V. R. Saunders, Chem. Phys. **156**, 11 (1991).
[27] *CRC Handbook of Chemistry and Physics*, 79th ed., edited by David R. Lide (CRC Press, Boca Raton, FL 1998).
[28] K. R. Tsai, P. M. Harris, and E. N. Lassettre, J. Phys. Chem. **60**, 338 (1956).